Magnetism of Co-doped ZnO epitaxially grown on a ZnO substrate

Li Li,[1] Y. Guo,[2,*] X. Y. Cui,[1] Rongkun Zheng,[1,†] K. Ohtani,[2] C. Kong,[3] A. V. Ceguerra,[1] M. P. Moody,[1] J. D. Ye,[4] H. H. Tan,[4] C. Jagadish,[4] Hui Liu,[5] C. Stampfl,[6] H. Ohno,[2,7,8] S. P. Ringer,[1] and F. Matsukura[2,7,8,‡]

[1]*Australian Center for Microscopy & Microanalysis, The University of Sydney, Sydney, 2006 NSW, Australia*

[2]*Laboratory for Nanoelectronics and Spintronics, Research Institute of Electrical Communication, Tohoku University, Katahira 2-1-1, Aoba-ku, Sendai 980-8577, Japan*

[3]*Electron Microscope Unit, University of New South Wales, Sydney, 2052 NSW, Australia*

[4]*Department of Electronic Materials Engineering, Australian National University, Canberra, ACT 0200, Australia*

[5]*Department of Electronics, College of Information Technical Science, Nankai University, Tianjin 300071, China*

[6]*School of Physics, The University of Sydney, Sydney, 2006 NSW, Australia*

[7]*WPI-Advanced Institute for Materials Research (WPI-AIMR), Tohoku University, 2-1-1 Katahira, Aoba-ku, Sendai 980-8577, Japan*

[8]*Center for Spintronics Integrated System, Tohoku University, 2-1-1 Katahira, Aoba-ku, Sendai 980-8577, Japan*

(Received 19 April 2012; published 23 May 2012)

In order to unravel the magnetism of Co-doped ZnO films, we have performed rigorous experiments on Co-doped ZnO grown on O-polar ZnO $(000\bar{1})$ substrates by molecular beam epitaxy. We find that the ZnO:Co with Co composition less than 20% is paramagnetic even at low temperatures, whereas that with Co composition of 20% shows ferromagnetism at room temperature. Although an additional *n*-type doping with Ga increases the magnitude of magnetization, the origin of the observed ferromagnetism is not carrier induced, as confirmed by electric-field effect measurements. Three-dimensional atom probe tomography shows that Co ions are randomly distributed, indicating that Co clustering or spinodal decomposition is not the origin of the ferromagnetism either. One possible mechanism for the ferromagnetism is hydrogen-facilitated interaction, which is supported experimentally by magnetic measurements on hydrogen-treated ZnO:Co as well as theoretically by first-principles calculation.

DOI: 10.1103/PhysRevB.85.174430 PACS number(s): 75.50.Pp, 75.70.−i, 81.05.Dz, 61.72.sh

I. INTRODUCTION

Considered as one of the most promising candidates for future improvements in electronic devices, semiconductor spintronics integrate the logic-processing functionalities of semiconductors and the information-storage functionalities of magnetism in single elements.[1] Practical devices will require suitable room-temperature ferromagnetic semiconductors to allow the simultaneous control of the charge and spin states of electrons. Since the demonstration of ferromagnetism in III-V magnetic semiconductors (In,Mn)As and (Ga,Mn)As,[2,3] and the prediction of high-temperature ferromagnetism in wide-gap semiconductors,[4,5] a great amount of effort has been devoted to this research field to discover new room-temperature ferromagnetic semiconductors.[6–8] Co-doped ZnO (ZnO:Co) is the first ZnO-based room-temperature ferromagnetic semiconductor that was theoretically predicted and experimentally examined.[4,5,9] Despite being one of the most representative and extensively investigated wide-gap magnetic materials,[7] ZnO:Co lacks a clear explanation for its observed magnetism: Room-temperature ferromagnetism in ZnO:Co has been widely reported,[7,9–12] but paramagnetic or antiferromagnetic behavior has also been observed.[13–16] Speculation is rife as to the origin of the observed ferromagnetism, with proposals including electron-induced (or enhanced) ferromagnetism,[5,17–19] spinodal decomposition,[20] and defect-induced ferromagnetism through the formation of bound magnetic polarons,[21–25] as well as an extrinsic origin due to the precipitation of a second phase.[26,27] So far, single-crystal Al_2O_3 is the most widely used substrate for growing ZnO films, but the lattice mismatch between the epitaxial layer and substrates produces a large number of crystal defects,[28] which may hinder the intrinsic properties of ZnO-based magnetic semiconductors.

In this work, therefore, we performed a systematic investigation of the microstructural and magnetic properties of ZnO:Co grown on O-polar ZnO $(000\bar{1})$ substrates by oxygen radical plasma-assisted molecular beam epitaxy (PMBE).[29]

II. SAMPLE PREPARATION AND CHARACTERIZATIONS

The epitaxial growth of ZnO:Co was performed in a PMBE chamber, for which the growth condition has been well-established for undoped ZnO.[29] Metal fluxes were supplied by evaporating high-purity elements (7N zinc, 5N cobalt, and 7N gallium), and O flux was supplied in the form of active oxygen (6N) radicals by a radiofrequency (rf) radical cell equipped with an electrostatic ion trap. Throughout growth, the flow rates of O_2 and rf power were kept at 0.5 sccm and 300 W, respectively. The substrates used in this study were commercial double-face polished single-crystal ZnO $(000\bar{1})$ chips with an area of 10×10 mm^2 and thickness of 1 mm grown by hydrothermal method. The use of ZnO substrate can efficiently reduce the number of defects in ZnO:Co because of the similar lattice constant and thermal expansion coefficient between epitaxial layer and substrate. After degreasing by acetone and ethanol, ZnO substrate was *in situ* outgassed in an ultrahigh-vacuum PMBE chamber (10^{-9} Torr, without oxygen) at 850 °C for 30 min. Next, a 40-nm-thick low-temperature-grown ZnO buffer layer was grown at 400 °C and annealed at 850 °C for 15 min.

We grew a series of Co-doped ZnO layers with thickness of 10–40 nm; some samples were codoped with Ga to investigate the effect of the existence of mobile carriers. We define the Co and Ga compositions as $Zn_{1-x-y}Co_xGa_yO$, where x is determined by secondary ion mass spectroscopy, and y is from the electron concentration n measured by the Hall measurement at room temperature. In this work, x ranges from

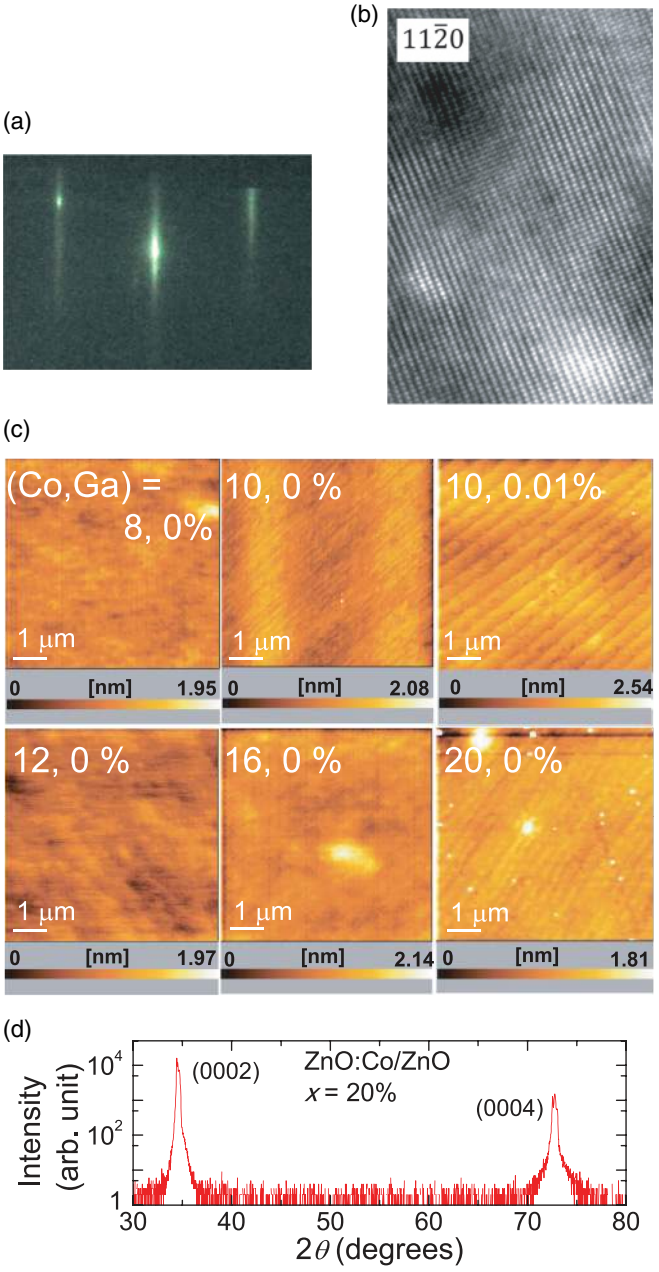

FIG. 1. (Color online) (a) A streaky reflection high-energy electron diffraction (RHEED) pattern for ZnO:Co on ZnO substrate. The picture is taken along $[\bar{1}120]$ azimuth for $Zn_{1-x}Co_xO$ with $x = 10\%$. (b) High-resolution transmission electron microscopy (HRTEM) image for $Zn_{1-x}Co_xO$ with $x = 20\%$ on ZnO substrate at operation voltage of 300 kV. (c) Atomic force microscopy images with area of 5×5 μm^2 for 40-nm-thick $Zn_{1-x-y}Co_xGa_yO$ with various sets of (x, y). (d) θ-2θ x-ray diffraction (XRD) for $Zn_{1-x}Co_xO$ with $x = 20\%$ on ZnO substrate. The curve is obtained by using Ni-filtered Cu Kα radiation.

8% to 20%, and y ranges from 0% to 0.01%. The growth front was monitored by reflection high-energy electron diffraction (RHEED), which shows a streaky pattern for a wurtzite single phase, as shown in Fig. 1(a). High-resolution transmission electron microscopy (HRTEM) reveals that we obtained high-quality single-crystalline films without observable defects, as shown in Fig. 1(b). Surface morphology of the films measured

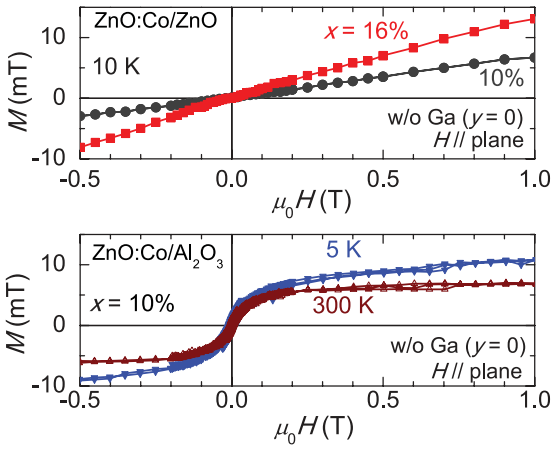

FIG. 2. (Color online) Magnetization curves of ZnO:Co under in-plane magnetic field. (a) $Zn_{1-x}Co_xO$ films grown on ZnO substrate with $x = 10\%$ and 16% show paramangetism at 10 K. (b) $Zn_{1-x}Co_xO$ film on Al_2O_3 substrate with $x = 10\%$ shows ferromagnetism at 300 K.

by atomic force microscope shows a flat surface with atomic monolayer steps, as shown in Fig. 1(c). X-ray diffraction (XRD) does not show any signature of the existence of the second phase within its detection limit, as shown in Fig. 1(d). We also prepared a $Zn_{1-x}Co_xO$ film with $x = 10\%$ on an a-Al_2O_3 substrate as a reference, which was grown under virtually the same growth condition as that on ZnO substrate.

III. THE EFFECTS OF SUBSTRATES

Figures 2(a) and 2(b) show in-plane magnetic field (H) dependence of magnetization (M) for 40-nm-thick ZnO:Co grown on ZnO and Al_2O_3 substrate, respectively, where magnetization from substrate is subtracted. The magnetization of the substrates is determined by a separate measurement, which shows diamagnetism with no detectable ferromagnetic response. The films with $x \leqslant 16\%$ on ZnO substrate are paramagnetic down to 10 K, with their susceptibilities almost proportional to x. On the other hand, the film with $x = 10\%$ on Al_2O_3 exhibits ferromagnetism at 300 K, suggesting that the observed ferromagnetism is related to crystal defects. The room-temperature Hall measurements also confirm the effects of the substrate. The films on ZnO are highly resistive, with n less than 10^{15} cm^{-3}, while that on Al_2O_3 has $n = 2 \times 10^{18}$ cm^{-3}. This high value of n is likely due to shallow donor defects, such as oxygen vacancies and zinc interstitials.

IV. THE EFFECTS OF Ga DOPING

In order to examine how charge carriers influence the magnetism of ZnO:Co, we codoped ZnO:Co on ZnO with n-type dopant Ga to obtain n comparable to that in ZnO:Co on Al_2O_3. Figure 3 shows the M-H curves at 10 K for the codoped $Zn_{1-x-y}Co_xGa_yO$ with $x = 10\%$ and $y = 0, 0.004\%$ ($n = 1.7 \times 10^{18}$ cm^{-3}), and 0.01% ($n = 4.2 \times 10^{18}$ cm^{-3}), where n is the free-electron concentration. The samples show paramagnetism, and their susceptibilities increase with increasing y, indicating that codoping with Ga enhances the M

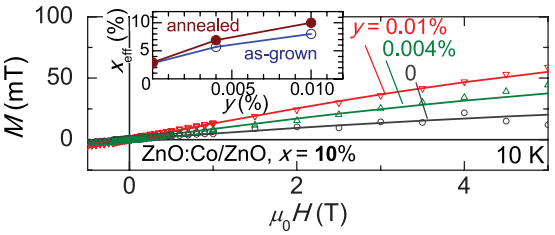

FIG. 3. (Color online) Magnetization curves of $Zn_{1-x}Co_xO$/ZnO with $x = 10\%$ at 10 K. $Zn_{1-x}Co_xO$/ZnO with $x = 10\%$ shows paramagnetism. Symbols are experimental data, and solid lines are fits by the Brillouin function. The magnetization increases with the increase of codoped Ga composition y. The inset shows the effective Co composition x_{eff} determined by the fits as a function of y for as-grown and annealed samples.

of ZnO:Co. The effective Co composition (x_{eff}) participating in magnetism is determined by fitting to M-H curves using the Brillouin function (solid curves in Fig. 3) under the assumption that the magnetic moment per Co atom is $3\mu_B$ (μ_B: Bohr magneton). As shown in the inset of Fig. 3, x_{eff} increases with y. After the annealing at 750 °C for 5 min in a vacuum, the magnetization is further enhanced, and x_{eff} reaches the nominal x of 10% with the samples codoped with Ga of 0.01%. However, ferromagnetism is not observed down to 10 K. Therefore, the observed ferromagnetism in the ZnO:Co on Al_2O_3 substrate is not carrier induced but is probably defect induced, as proposed in the framework of the bound magnetic polarons model or due to the Co precipitates.[21–25]

V. FERROMAGNETIC ZnO:Co WITH $x = 20\%$

As shown by the M-H curves in Fig. 4, when x is increased to 20%, the ferromagnetism in ZnO:Co on the ZnO substrate can be observed even at room temperature. It shows a clear ferromagnetic hysteresis loop with paramagnetic response at higher magnetic fields. The temperature dependence of M shows that the Curie temperature is beyond 400 K. The observed ferromagnetism at higher x may be related to the establishment of a magnetic-interaction percolation path,[19] because the magnetic coupling among Co spins is expected to be short-ranged.[30,31] The magnitude of the magnetization can be increased again by codoping with Ga. These results prompt questions about the effects of Ga doping, since it is known that carrier doping has two effects: the effects

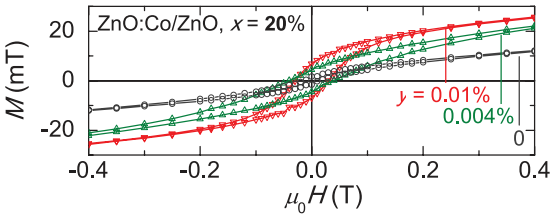

FIG. 4. (Color online) Magnetization curves of $Zn_{1-x}Co_xO$/ZnO with $x = 20\%$ at 300 K. $Zn_{1-x}Co_xO$/ZnO with $x = 20\%$ shows ferromagnetism at 300 K with background paramagnetic response. The magnitude of magnetization increases with the increase of codoped Ga composition y, similar to Fig. 3.

on magnetic interaction (free-carrier mediated interaction or double-exchange interaction) and Co ion aggregation.[17,18,32,33] Our experiments demonstrate that Ga codoping enhanced the magnetization of both paramagnetic $Zn_{1-x}Co_xO$ with $x = 10\%$ and ferromagnetic $Zn_{1-x}Co_xO$ with $x = 20\%$, but it does not induce ferromagnetic interaction in paramagnetic $Zn_{1-x}Co_xO$ with $x = 10\%$.

VI. THE EFFECTS OF ELECTRIC FIELD

In order to further explore the influence on the magnetism of n, we fabricated metal-insulator-semiconductor (MIS) structures to control n through gate electric fields, V_G.[34–37] Fabrication of MIS structure consists of five steps, etching of the semiconductor, deposition of an ohmic electrode, deposition of an insulator, etching of the insulator, and deposition of the gate electrode. First the ZnO:Co layer is etched by using $HCl:H_3PO_4:H_2O$ (0.5:0.5:1000) to form a large square mesa with area about 6 mm^2 for M measurements or a Hall-bar–shaped mesa with a 30-μm-wide and 200-μm-long channel for transport measurements. After deposition of the ohmic electrodes (10 nm Ti/30 nm Al/50 nm Au), the sample is introduced into an atomic layer deposition (ALD) chamber and a 50-nm-thick Al_2O_3 gate insulator is deposited at 150 °C by applying alternative pulses of $Al(CH_3)_3$ and H_2O with N_2 purges between each step. In order to remove the insulator above the ohmic electrodes, the sample is dipped in etchant $HF:NH_4F:H_2O$ (1:10:10) for 5 min. Finally, a 5 nm Cr/100 nm Au gate electrode is deposited and lifted off.

The conductivity of the Ga-codoped ZnO:Co channel with $n = 4 \times 10^{18}$ cm^{-3} can be modulated approximately up to 40% by the application of $V_G = 8$ V, which corresponds to an electric field of 1.6 MV/cm [the inset of Fig. 5(b)]. Figure 5 shows M-H curves under V_G on (a) a paramagnetic sample with $x = 5\%$ and $y = 0.01\%$ at 300 K and (b) a

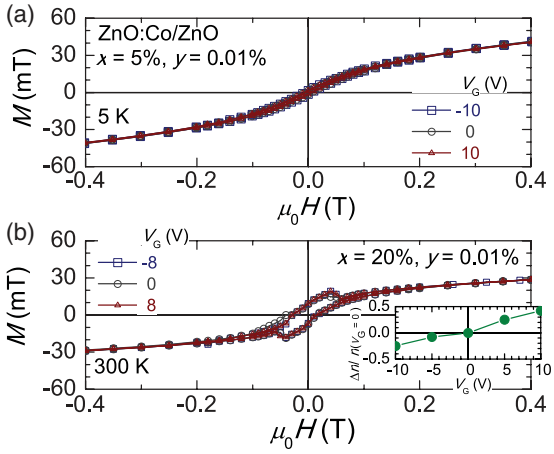

FIG. 5. (Color online) Gate voltage dependence of magnetization curves for ZnO:Co/ZnO. (a) Paramagnetic $Zn_{1-x-y}Co_xGa_yO$ with $x = 5\%$ and $y = 0.01\%$ measured at 5 K. (b) Ferromagnetic $Zn_{1-x-y}Co_xGa_yO$ with $x = 20\%$ and $y = 0.01\%$ measured at 300 K. Magnetization of both ZnO:Co does not show any influence of gate voltage V_G and thus electron concentration n. The inset shows the relative change in n, $\Delta n/n(V_G = 0)$, by the application of V_G, which is determined by transport measurements at room temperature.

ferromagnetic sample with $x = 20\%$ and $y = 0.01\%$ at 300 K (the distorted shape in the hysteresis is due to the nonuniform in-plane geometry associated with the MIS structure).[38] The M-H curves do not show any clear dependence of V_G despite of the relatively large change in n. This behavior is very different from the well-established carrier-mediated ferromagnetic semiconductors, such as (Ga,Mn)As,[37] which show a clear dependence of magnitude of magnetization on V_G. The results indicate that carrier doping during growth influences the magnetism on ZnO:Co, but such a change in n does not affect the magnetism once the material is fabricated.

VII. ATOM PROBE TOMOGRAPHY

It has been suggested that nanospinodal decomposition is linked to the observed ferromagnetism in ZnO:Co.[20] All of the conventional structural-analysis techniques (RHEED, XRD, and HRTEM; see Fig. 1) utilized in this work reveal that the films are high-quality single crystals without observable defects or heterogeneities. It is known that three-dimensional (3D) atom probe tomography (APT) has the capability to map the chemical identity and 3D positions of individual atoms with single-atom depth resolution and subnanometer lateral resolution.[39] Therefore, we adopted APT to measure Co distribution in $Zn_{1-x}Co_xO$ with $x = 20\%$.[40,41] The fabrication of the atom probe tip was performed using a dual-beam scanning electron microscope and focused ion beam instrument with a Ga-ion beam accelerated at 30 keV.[42] The final step of tip preparation was a low-energy annular cleaning mill at 5 keV to remove Ga implantation and damage from the ion beam. The APT was performed with a wide-field-of-view atom probe at 20 K in an ultrahigh-vacuum chamber at a pressure of $\sim 2 \times 10^{-11}$ Torr. Voltage pulses were used to field evaporate the atoms from the tip, at a pulse fraction of 25%.

The APT mass spectrum for $Zn_{1-x}Co_xO$ with $x = 20\%$ on ZnO is shown in Fig. 6(a), where chemical identities were determined by time-flight-mass spectroscopy. The APT data set was first divided into blocks containing a certain number of atoms (here 100 atoms are used) to produce a contingency table as shown in Table I, where "+" indicates that the experimental value is greater than the expected value, and "−" indicates the opposite. Contingency analysis determines whether two species are more likely to be found within the same block as one another, thus forming a picture of whether the two solute species are cosegregated or antisegregated.

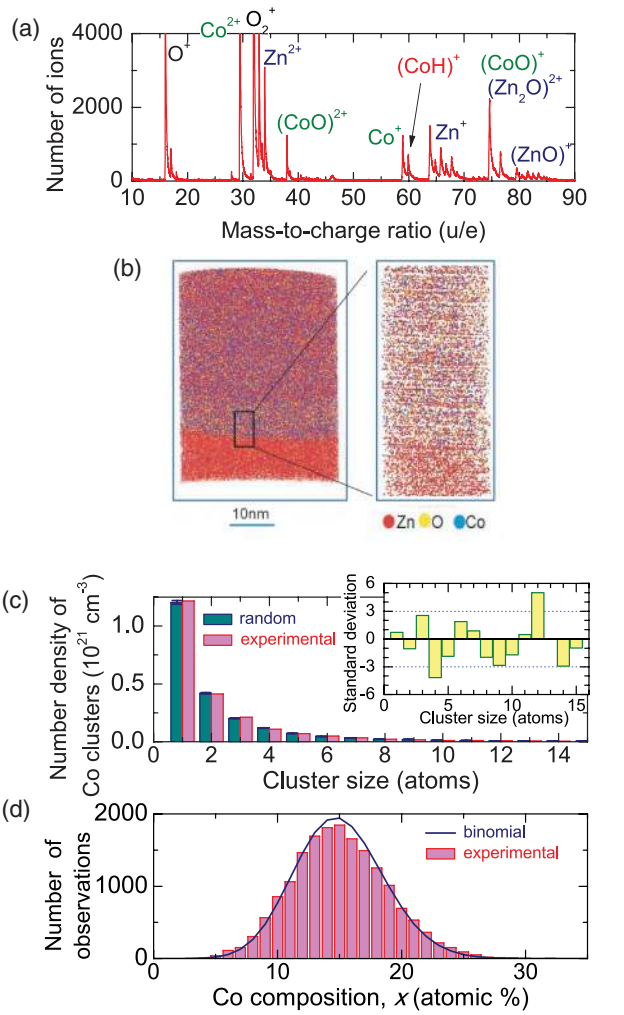

FIG. 6. (Color online) (a) Mass spectrum from atom probe tomography (ATP) for $Zn_{1-x}Co_xO$ with $x = 20\%$ on ZnO substrate. (b) Three-dimensional ATP reconstruction; each dot represents a single atom of Zn, O, and Co. (c) Experimental number density of Co clusters compared to the random number density obtained by 3D Markov field algorithm analysis. The inset is the significance of the difference between the experimental and the random data (the number of standard deviation). (d) Frequency distribution of the Co compositions measured in 100-ion blocks is very close to the corresponding random distribution (binomial distribution) shown by the solid line.

TABLE I. Contingency table analysis for Zn and Co for $Zn_{1-x}Co_xO$ with $x = 20\%$ on ZnO substrate.

	Number of Zn atoms						
Number of Co atoms	0 – 44	45 – 49	50 – 54	55 – 59	60 – 64	65 – 69	70 – 100
0 – 4	−	−	−	−	−	+	+
5 – 9	−	−	−	−	+	+	+
10 – 14	−	−	−	−	+	+	+
15 – 19	−	−	+	+	−	−	−
20 – 24	−	+	+	+	−	−	−
25 – 29	+	+	+	−	−	−	−
30 – 100	+	+	−	−	−	−	−

TABLE II. Contingency table analysis for H and Co for $Zn_{1-x}Co_xO$ with $x = 20\%$ on ZnO substrate.

	Number of H atoms						
Number of Co atoms	0 – 15	15 – 20	20 – 25	25 – 30	30 – 35	35 – 40	40 – 100
0 – 10	+	+	+	−	−	−	−
10 – 15	+	+	+	+	−	−	−
15 – 20	−	−	−	+	+	+	+
20 – 25	−	−	−	+	+	+	+
25 – 100	−	−	−	−	+	+	+

Table I shows clearly that Zn and Co atoms are antisegregated, suggesting strongly that Co atoms substitute into Zn cation sites. Then, a 3D reconstruction of the atom distributions in Fig. 6(b) was generated from a data set of more than 10 million atoms, in which a single Zn, O, and Co atom is each presented by colored dots, indicating Zn, O, and Co. While the wurtzite ZnO (0002) planes are clearly resolved, neither precipitates nor spinodal decomposition is visually apparent. In order to examine quantitatively the distribution of Co atoms, we applied a number of analytical approaches, which include 3D Markov field and frequency distribution analyses.[43,44] The 3D Markov field approach constitutes a solute cluster-identification technique.[43] It tests the hypothesis that the solute is randomly distributed by measuring the difference between experimentally observed clusters and their distribution for random arrangement of the solute. As shown in Fig. 6(c), there is only a slight difference between the observed distribution of clusters and the standard random distribution, indicating that the Co atoms are distributed randomly in the ZnO matrix. The biggest cluster comprises only 15 atoms, which cannot be a source of ferromagnetism at room temperature. This conclusion is supported by the frequency distribution analysis as shown in Fig. 6(d),[44] where the frequency distribution of the Co concentration measured in blocks of 100 atoms is compared with the theoretical binomial distribution. The agreement in experimental and binomial distribution confirms again that the Co dopants are distributed randomly in the ZnO matrix, ruling out clustering and spinodal decomposition. The results of APT on a sample codoped with Ga ($y = 0.01\%$) give essentially the same result, indicating the Ga doping does not influence the Co atom distribution in ZnO:Co.

We see that the observed ferromagnetism in ZnO:Co on ZnO is not related to carrier-mediated interaction, spinodal decomposition, precipitates, and defect-induced bound magnetic polaron. Superexchange coupling is likely to be antiferromagnetic,[20,31] which is not expected to be the origin of the ferromagnetism. Therefore, the origin of the ferromagnetism in ZnO:Co on ZnO is mysterious, especially the observed effect on magnetism of Ga or electron doping.

VIII. THE ROLE OF HYDROGEN

Finally, we focus on the effect of unintentionally doped impurity hydrogen in ZnO:Co, because the APT mass spectrum of ZnO:Co clearly shows a Co-H dimer peak [see Fig. 6(a)]. Contingency table analysis in Table II indicates that Co and H atoms are cosegregated. Hydrogen is known to be an important unintentionally introduced impurity in ZnO,[45–47] and it has been discussed as an efficient agent to couple Co spins ferromagnetically.[48–54] The secondary ion mass spectroscopy (SIMS) measurements also show the existence of H in the samples, and H concentration in $Zn_{1-x}Co_xO$ with $x = 20\%$ is one order higher than that with $x = 16\%$, as shown in Fig. 7. The difference in H concentration may be related to the difference in magnetism. In order to test the effects of H doping, 10% of elemental H was introduced to a few paramagnetic samples by a plasma treatment in an inductively coupled plasma reacting ion etching (ICP-RIE) system. The treatment was done at 180 °C for 60 min with H_2 flow rate of 30 sccm; the ICP and RIE powers were 1 kW and 5 W, respectively. During plasma treatment, the samples were put on Si substrate to avoid the possible introduction of magnetic impurities. We measured the *M-H* curve of H-treated ZnO substrate, which shows diamagnetism and no effect of H on the magnetism of ZnO substrate. Figure 8 shows the *M-H* curves of $Zn_{1-x}Co_xO$ with $x = 16\%$ after the introduction of H, which shows room-temperature ferromagnetism, indicating an important role of H in inducing ferromagnetism. The *M-H* curve at 300 K shows smaller coercivity but larger magnetization than that of $Zn_{1-x}Co_xO$ with $x = 20\%$ and without H, shown in Fig. 4. There also seems to be a superparamagnetic component after H treatment. These differences in magnetic behaviors indicate the difference between the H introduction by plasma treatment in the $Zn_{1-x}Co_xO$ with $x = 16\%$ and the unintentional incorporation of H in the $Zn_{1-x}Co_xO$ with $x = 20\%$. In the former case, H introduced by plasma treatment

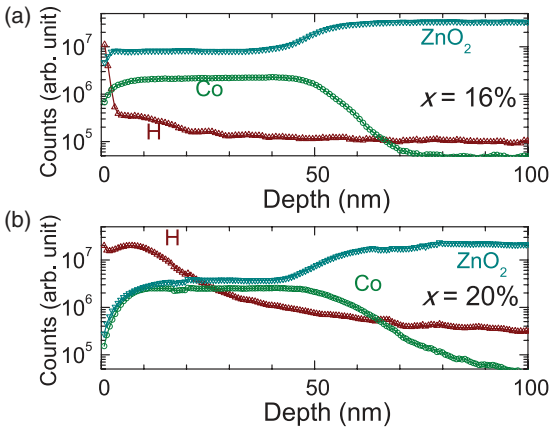

FIG. 7. (Color online) Secondary ion mass spectroscopy (SIMS) profiles of Zn, Co, and H elements in $Zn_{1-x}Co_xO$ on ZnO substrate with (a) $x = 16\%$ and (b) $x = 20\%$.

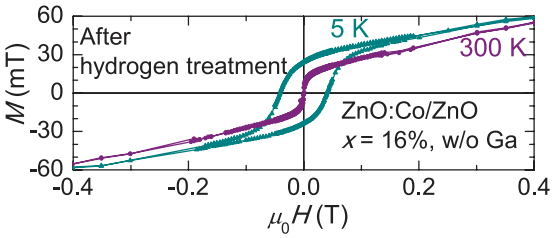

FIG. 8. (Color online) Magnetization curves of $Zn_{1-x}Co_xO$/ZnO with $x = 16\%$ after hydrogen treatment.

penetrated deeper and may result in structural defects in the ZnO:Co matrix. The nonuniform distribution of H and the possible structural defects may lead to superparamagnetic clusters and smaller coercivity at 300 K. The latter case, where the H concentrates on the surface, has a smaller magnetization.

We performed first-principles calculations based on density functional theory using the generalized gradient approximation[55] with the DMol^3 code.[56] We assume that the H atoms are interstitial rather than substitutional, in line with the experimental observations.[50] By comparing the total energy of configurations with Co atoms on different sites in a 32-atom supercell, shown in Fig. 9, we find that it is energetically favorable for H to associate with Co atoms, and the two most favorable configurations are those where the H atoms reside at the Co-O bond center (BC) sites, namely $BC_{\parallel}$ and $BC_{\perp}$ (Table III). This is consistent with the Co-H dimers that are observed in the ATP mass spectra in Fig. 6(a) and with the cosegregation trend of Co and H atoms from contingency table analysis in Table II. Given the abundance and high mobility of H, the attraction between these two types of atoms gives a natural explanation of the spontaneous diffusion of H into ZnO:Co. It is noteworthy that the presence of H at the most favorable site, $BC_{\perp}$, blocks the diffusion pathway along the [0001] epitaxial growth direction, such that the concentration of unintentionally doped H will rapidly decrease with the depth of thin film, as observed in the SIMS measurements. The simulation of Co-Co magnetic interaction in ZnO:Co without and with H was performed in a 16-atom cell that contains two

TABLE III. Total energy (in meV) of H-doped ZnO and ZnO:Co relative to the most favorable configurations.

	$AB_{\parallel}$	$AB_{\perp}$	$BC_{\parallel}$	$BC_{\perp}$	Far-$BC_{\parallel}$	Far-$BC_{\perp}$
ZnO	156.6	249.4	0	141.0	–	–
ZnO:Co	713.6	429.2	120.3	0	456.0	617.8

substitutional Co atoms in different configurations, i.e., with the concentration of the Co doping being 25%. Without H, the two most favorable structures are Co atoms that form an in-plane pair and then an out-of-plane pair. For both cases, the antiferromagnetic state is the ground state with atomic spin moment of $\sim 2.5\mu_B$ [Figs. 10(a) and 10(b)]. We then introduced one or two H atoms at various locations into each Co-pair configuration and generated the spin-density isosurface plots for the energetically favorable configurations as shown in Fig. 10. As seen clearly in Figs. 10(b) and 10(d), a single H atom can mediate the coupling between Co atoms, where a strong local ferromagnetic interaction of approximately 100 meV per Co atom is observed and the introduction of a H atom changes the atomic moment of the nearest Co to $1.9\mu_B$. With two H atoms, the favorable structures are also ferromagnetic, with a stronger interaction of $\sim$150 meV per Co atom over the antiferromagnetic coupling. Larger Co atom separations (0.463 nm or 0.530 nm simulated in a 32-atom cell) produce a weak interaction below 5 meV per Co atom, regardless of the presence of H. Such short range of the magnetic interaction implies that, for randomly distributed Co, H can mediate high-temperature ferromagnetism only in ZnO:Co with a high Co concentration, in agreement with the previous predictions and the present observation.[53,57]

IX. SUMMARY

In summary, we have investigated magnetic properties of Co-doped ZnO on ZnO substrate grown by molecular beam epitaxy. The sample with Co composition of 20% exhibits ferromagnetism at room temperature, and those with doping concentration below 16% shows paramagnetism, even

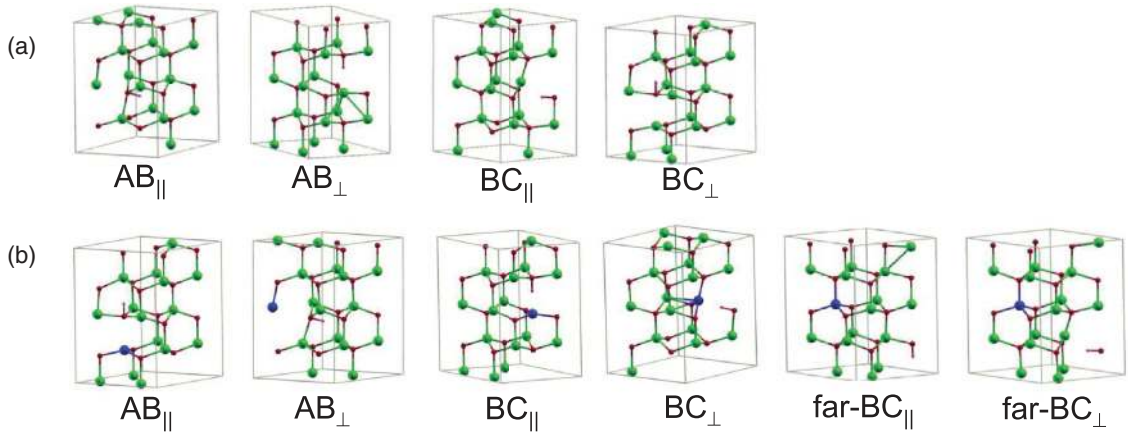

FIG. 9. (Color online) Possible configurations of one H atom in (a) ZnO matrix and (b) ZnO matrix containing one Co atom, where Zn, O, Co, and H atoms are denoted as large green, small red, large blue, and small pink spheres, respectively.

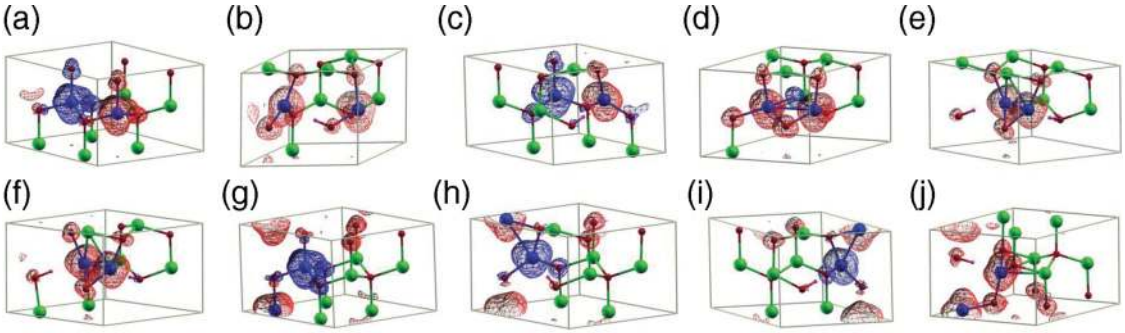

FIG. 10. (Color online) Calculated isosurfaces of spin density for various energetically favourable configurations containing pair of Co atoms in ZnO with and without H atoms using a 16-atom supercell. (a), (g) Without H. (b)-(d), (h)-(j) With one H atom. (e), (f) With two H atoms. Red and blue isosurfaces present positive and negative spin polarization, respectively. Isosurface value is 0.03 electrons/Å^3. Zn, O, Co, and H atoms are denoted as large green, small red, large blue, and small pink spheres, respectively.

at low temperatures. While Ga donor codoping enhances the magnetization, the modulation of electron concentration by electric fields does not affect the magnetic properties, indicating that the observed ferromagnetism is not related to a carrier-induced mechanism. The careful structural analyses show that there are no observable defects, precipitates, or spinodal decomposition. We have confirmed that the introduction of hydrogen can induce the ferromagnetism of ZnO:Co at room temperature. The unintentionally introduced H may have nontrivial effects on ZnO-based magnetic semiconductors. Room-temperature ferromagnetic semiconductors with good reproducibility in synthesis and an understanding of the origin of ferromagnetism are very significant but very challenging. The present results show that the magnetism of ZnO:Co depends strongly on the numbers of crystal defects and impurities. For further understanding the intrinsic properties of ferromagnetic semiconducting materials, the control of sample quality is crucial.

ACKNOWLEDGMENTS

The authors thank Kyle Ratinac, Wai Kong Yeoh, Leigh Stephenson, Baptiste Gault, Mohamed Belmoubarik, Maciej Sawicki, and Tomasz Dietl for discussion, and Lutao Weng for SIMS experiments. The authors acknowledge the facilities of, and technical assistance from staff at, the Australian Microscopy & Microanalysis Research Facility (AMMRF) at the University of Sydney, the University of New South Wales, the University of Adelaide, and Australian National Computational Infrastructure (NCI). This work was supported in part by the Australian Research Council (DP0770987), by the Japan Society for the Promotion of Science (JSPS) through its "Funding Program for World-Leading Innovative R & D on Science and Technology (FIRST program)," by Exploratory Research for Advanced Technology (ERATO), Japan Science and Technology Corporation (JST), and by the Global Center of Excellence (GCOE) programs at Tohoku University.

*Present address: Beijing National Laboratory for Condensed-Matter Physics and Institute of Physics, Chinese Academy of Sciences, Beijing 100190, China.
†Corresponding author: rongkun.zheng@sydney.edu.au
‡f-matsu@wpi-aimr.tohoku.ac.jp

[1]D. D. Awschalom and M. E. Flatte, Nature Physics **3**, 153 (2007).
[2]H. Ohno, H. Munekata, T. Penney, S. von Molnár, and L. L. Chang, Phys. Rev. Lett. **68**, 2664 (1992).
[3]H. Ohno, A. Shen, F. Matsukura, A. Oiwa, A. Endo, S. Katsumoto, and Y. Iye, Appl. Phys. Lett. **69**, 363 (1996).
[4]T. Dietl, H. Ohno, F. Matsukura, J. Cibert, and D. Ferrand, Science **287**, 1019 (2000).
[5]K. Sato and H. Katayama-Yoshida, Jpn. J. Appl. Phys., Part 2 **40**, L334 (2001).
[6]S. A. Chambers, Surf. Sci. Rep. **61**, 345 (2006).
[7]F. Pan, C. Song, X. J. Liu, Y. C. Yang, and F. Zeng, Mater. Sci. Eng., R **62**, 1 (2008).
[8]T. Dietl, Nat. Mater. **9**, 965 (2010).
[9]K. Ueda, H. Tabata, and T. Kawai, Appl. Phys. Lett. **79**, 998 (2001).
[10]J. H. Kim, H. Kim, D. Kim, Y. E. Ihm, and W. K. Choo, J. Appl. Phys. **92**, 6066 (2002).
[11]A. J. Behan, A. Mokhtari, H. J. Blythe, D. Score, X.-H. Xu, J. R. Neal, A. M. Fox, and G. A. Gehring, Phys. Rev. Lett. **100**, 047206 (2008).
[12]Z. L. Lu, H. S. Hsu, Y. H. Tzeng, F. M. Zhang, Y. W. Du, and J. C. A. Huang, App. Phys. Lett. **95**, 102501 (2009).
[13]M. H. Kane, K. Shalini, C. J. Summers, R. Varatharajan, J. Nause, C. R. Vestal, Z. J. Zhang, and I. T. Fergunson, J. Appl. Phys. **97**, 023906 (2005).
[14]N. Jedrecy, H. J. von Bardeleben, Y. Zheng, and J.-L. Cantin, Phys. Rev. B **69**, 041308(R) (2004).
[15]G. Lawes, A. S. Risbud, A. P. Ramirez, and R. Seshadri, Phys. Rev. B **71**, 045201 (2005).
[16]M. S. Moreno, T. Kadama, R. E. Dunin-Borkowski, D. Cooper, P. A. Midgley, L. B. Steren, S. Duhalde, and M. F. Vignolo, J. Phys. D: Appl. Phys. **39**, 1739 (2006).
[17]X. H. Xu, H. J. Blythe, M. Ziese, A. J. Behan, J. R. Neal, A. Mokhtari, R. M. Ibrahim, A. M. Fox, and G. A. Geharing, New J. Phys. **8**, 135 (2006).

[18]A. Walsh, J. L. F. Da Silva, and S.-H. Wei, Phys. Rev. Lett. **100**, 256401 (2008).
[19]S. Lany, H. Raebiger, and A. Zunger, Phys. Rev. B **77**, 241201(R) (2008).
[20]T. Dietl, T. Andrearczyk, A. Lipinska, M. Kiecana, M. Tay, and Y. Wu, Phys. Rev. B **76**, 155312 (2007).
[21]J. M. D. Coey, M. Venkatesean, and B. C. Fitzferald, Nat. Mater. **4**, 173 (2005).
[22]C. H. Patterson, Phys. Rev. B **74**, 144432 (2006).
[23]M. Gacic, G. Jakob, C. Herbort, H. Adrian, T. Tietze, S. Bruck, and E. Goering, Phys. Rev. B **75**, 205206 (2007).
[24]T. Tietze, M. Gacic, G. Schütz, G. Jakob, S. Brück, and E. Goering, New J. Phys. **10**, 055009 (2008).
[25]N. H. Hong, A. Barla, J. Sakai, and N. Q. Huong, Phys. Status Solidi C **4**, 4461 (2007).
[26]J. H. Park, M. G. Kim, H. M. Jang, S. Ryu, and Y. M. Kim, Appl. Phys. Lett. **84**, 1338 (2004).
[27]N. Jedrecy, H. J. von Bardeleben, and D. Demaille, Phys. Rev. B **80**, 205204 (2009).
[28]C. Song, F. Zeng, K. W. Geng, X. J. Liu, F. Pan, B. He, and W. S. Yan, Phys. Rev. B **76**, 045215 (2007).
[29]H. Xu, K. Ohtani, M. Yamao, and H. Ohno, Appl. Phys. Lett. **89**, 071918 (2006).
[30]K. Sato, H. Katayama-Yoshida, and P. H. Dederichs, Jpn. J. Appl. Phys., Part 2 **44**, L948 (2005).
[31]E.-C. Lee and K. J. Chang, Phys. Rev. B **69**, 085205 (2004).
[32]T. Dietl, Nat. Mater. **5**, 673 (2006).
[33]S. Kuroda, N. Nishizawa, K. Takita, M. Mitome, Y. Bando, K. Osuch, and T. Dietl, Nat. Mater. **6**, 440 (2007).
[34]H. Ohno, D. Chiba, F. Matsukura, T. Omiya, E. Abe, T. Dietl, Y. Ohno, and K. Ohtani, Nature **408**, 944 (2000).
[35]D. Chiba, F. Matsukura, and H. Ohno, Appl. Phys. Lett. **89**, 162505 (2006).
[36]H. J. Lee, E. Helgren, and F. Hellman, Appl. Phys. Lett. **94**, 212106 (2009).
[37]M. Sawicki, D. Chiba, A. Korbecka, Y. Nishitani, J. A. Majewski, F. Matsukura, T. Dietl, and H. Ohno, Nature Phys. **6**, 22 (2010).
[38]P. Stamenov and J. M. D. Coey, Rev. Sci. Instrum. **77**, 015106 (2006).
[39]R. K. Zheng, M. P. Moody, B. Gault, Z. W. Liu, H. Liu, and S. P. Ringer, J. Magn. Magn. Mater. **321**, 935 (2009).
[40]M. Kodzuka, T. Ohkubo, K. Hono, F. Matsukura, and H. Ohno, Ultramicroscopy **109**, 644 (2009).
[41]R. Lardé, E. Talbot, F. Vurpillot, P. Pareige, G. Schmeber, E. Beaurepaire, A. Dinia, and V. Pierron-Bohnes, J. Appl. Phys. **105**, 126107 (2009).
[42]M. K. Miller, K. F. Russell, and G. B. Thompson, Ultramicroscopy **102**, 287 (2005).
[43]A. V. Ceguerra, M. P. Moody, L. T. Stephenson, R. K. W. Marceau, and S. P. Ringer, Philos. Mag. **90**, 1657 (2010).
[44]M. P. Moody, L. T. Stephenson, A. V. Ceguerra, and S. P. Ringer, Microscopy Res. Tech. **71**, 542 (2008).
[45]C. G. Van de Walle, Phys. Rev. Lett. **85**, 1012 (2000).
[46]S. F. J. Cox, E. A. Davis, S. P. Cottrell, P. J. C. King, J. S. Lord, J. M. Gil, H. V. Alberto, R. C. Vilão, J. Piroto Duarte, N. Ayres de Campos, A. Weidinger, R. L. Lichti, and S. J. C. Irvine, Phys. Rev. Lett. **86**, 2601 (2001).
[47]D. M. Hofmann, A. Hofstaetter, F. Leiter, H. Zhou, F. Henecker, B. K. Meyer, S. B. Orlinskii, J. Schmidt, and P. G. Baranov, Phys. Rev. Lett. **88**, 045504 (2002).
[48]H.-J. Lee, C. H. Park, S.-Y. Jeong, K.-J. Yee, C. R. Cho, M.-H. Hung, and D. J. Chadi, Appl. Phys. Lett. **88**, 062504 (2006).
[49]S. Lee, Y. C. Cho, S.-J. Kim, C. R. Cho, S.-Y. Jeong, S. J. Kim, J. P. Kim, Y. N. Choi, and J. M. Sur, Appl. Phys. Lett. **94**, 212507 (2009).
[50]S. J. Kim, S. Lee, Y. C. Cho, Y. N. Choi, S. Park, I. K. Jeong, Y. Kuroiwa, C. Moriyoshi, and S.-Y. Jeong, Phys. Rev. B **81**, 212408 (2010).
[51]S. Denka and P. A. Joy, Appl. Phys. Lett. **89**, 032508 (2006).
[52]Y. C. Cho, S.-J. Kim, S. Lee, S. J. Kim, C. R. Cho, H.-H. Nahm, C. H. Park, I. K. Jeong, S. Park, T. E. Hong, S. Kuroda, and S.-Y. Jeong, Appl. Phys. Lett. **95**, 172514 (2009).
[53]C. H. Park and D. J. Chadi, Phys. Rev. Lett. **94**, 127204 (2005).
[54]E.-Z. Liu, J. Magn. Magn. Mater. **321**, 3507 (2009).
[55]J. P. Perdew, K. Burke, and M. Ernzerhof, Phys. Rev. Lett. **78**, 1396 (1997).
[56]B. Delley, J. Chem. Phys. **113**, 7756 (2000).
[57]E.-C. Lee and K. J. Chang, Phys. Rev. B **69**, 085205 (2004).